IGSHPA Research Track
Las Vegas, December 6-8, 2022

Forecasting Hydraulic Head Changes in Injection Wells Using LSTM Network

Christopher Rose **Philippe Pasquier** **Alain Nguyen** **Gabrielle Beaudry**

ABSTRACT

Monitoring of well's specific capacity is commonly used to plan maintenance of injection wells in open-loop GSHP and standing column well systems. However, this method does not consider the effect of temperature on hydraulic conductivity. A first step towards an alternative approach that does include the effect of temperature is proposed in this work. We present a long short-term memory network capable of predicting the water level in the injection well of an operating GSHP system. The methodology consists of building a training set using a numerical model. A total of 500 simulations were conducted to evaluate hydraulic head signals under various inlet temperatures and flow rates along with hydraulic and thermal parameters drawn from a uniform distribution. Predictive performance of the artificial neural network is tested on an operational data set. The resulting RMSE between the forecasted and operational data set is 14.8 cm.

INTRODUCTION

Open-loop ground source heat pump (GSHP) and standing column well (SCW) systems are often used with injection wells (IW). Indeed, reinjecting pumped groundwater back to the aquifer allows maintaining the well's sustainability along with limiting the impact on the piezometric surface caused by continuously extracting groundwater (Banks, 2012; Snijders and Drijver, 2016). In SCW systems, discharging a fraction of the pumped groundwater in IWs induces a drawdown in SCWs, thus increasing groundwater flow towards SCWs. This bleed amplifies advection, which in turn contributes in stabilizing groundwater temperature entering the GSHP and temporarily boosting the SCW's thermal efficiency (Pasquier *et al.*, 2016).

However, IWs are also subject to fouling, clogging and overflowing problems along with degradation of performance (Banks, 2012). Forcing water into an IW can lodge gas bubbles, particles or chemical precipitates in fractures or pore spaces, thus reducing the hydraulic conductivity of the surrounding aquifer (Banks, 2012). Water dynamic viscosity, being temperature-dependent, also plays a role in altering hydraulic conductivity. Since hydraulic conductivity is inversely proportional to dynamic viscosity, injection capacity during winter months can be twice as low as the one observed in summer (Bouwer, 2002). Even though many precautionary measures can be carried out to minimize fouling problems, such as injecting below the water table, maintaining overpressure and preventing entry of oxygen, early redevelopment of IWs remains important to extend their remaining use of life as severely clogged wells might be difficult to restore (Snijders and Drijver, 2016). Monitoring the well's specific capacity through regular water level measurements can help to plan preventive maintenance of IWs (Ballard, 2017; Snijders and Drijver, 2016). An alternative surveillance method

Christopher Rose (christopher.rose@polymtl.ca) is an M.A.Sc. candidate at Polytechnique Montréal, Canada.
Philippe Pasquier (philippe.pasquier@polymtl.ca) is a professor of geological engineering at Polytechnique Montréal, Canada.
Alain Nguyen (tuananhalain.nguyen@NRCan-RNCan.gc.ca) is a research engineer at CanmetEnergy, Canada.
Gabrielle Beaudry (gabrielle.beaudry@polymtl.ca) is a research engineer at Polytechnique Montréal, Canada.

DOI: https://doi.org/10.22488/okstate.22.000024

for open-loop GSHP is based on a step-drawdown test performed during normal system operation to determine potential fouling and clogging issues (Gjengedal *et al.*, 2019). Although monitoring systems in GSHP applications can be easily implemented, accumulation of large data sets and a lack of hydrogeology expertise for data interpretation are some of the reported issues with these surveillance methods (Gjengedal *et al.*, 2018, 2021). A new approach, based on residual analysis between predicted and measured water level in the well, has potential to detect gradual decreases in infiltration capacity. The key to this approach is to accurately predict the water level in an efficient manner, that is including the effect of temperature on hydraulic conductivity and without the burden of running a computationally heavy numerical model for every prediction task.

Artificial neural networks (ANN) can tackle various prediction tasks with large data sets as they are able to learn complex non-linear relationship between input and output variables. Artificial intelligence is a thriving field with increasing applications in GSHP. The use of ANN now concerns GSHP coefficient of performance prediction (Cho *et al.*, 2021; Esen and Inalli, 2009; Puttige *et al.*, 2021; Sun *et al.*, 2015), ideal control strategies for GSHP systems (Wang *et al.*, 2020) and for hybrid GSHP systems (Gang *et al.*, 2014), modeling of borehole heat exchanger (Puttige *et al.*, 2020), construction of g-functions (Dusseault and Pasquier, 2018, 2019; Pasquier *et al.*, 2018), inference of thermal parameters (Pasquier and Marcotte, 2020), prediction of disturbed ground temperature (Zhou *et al.*, 2021) and financial optimization of GSHP systems (Dusseault and Pasquier, 2021). The previously mentioned ANN applications mostly involved feedforward neural networks and multi-layer perceptrons. Long short-term memory (LSTM) network, a kind of neural network using only sequential data for prediction, have yet to be widely used in GSHP even though being broadly employed in time series forecasting due to their fast and accurate prediction. LSTM networks represent a promising tool for GSHP systems as one can learn long-term dependencies, such as seasonality, and daily patterns. The use of LSTM networks in GSHP has to this day only been applied to prediction of building's thermal load demand (Xie *et al.*, 2020; Zhang *et al.*, 2020), detecting anomaly energy consumption (Xu and Chen, 2020), and forecasting indoor temperature (Xu *et al.*, 2019).

Residuals between forecasted and measured hydraulic head can act as a surrogate to fouling problems in IWs. However, we first need to rigorously predict the aquifer's response under different operating controls. This paper addresses this issue by demonstrating the potential of LSTM networks to forecast negative drawdown in the IW of a GSHP system and by validating the results with an operational data set. The methodology relies on a simplified 2D-axisymmetric finite-element model (FEM) to generate training and validation data sets that consider the crucial effect of temperature on hydraulic conductivity. To the best knowledge of the authors, it is the first LSTM network used to predict water level variations of an operating IW using only a FEM at training and validation steps. Weights and biases of the different hidden layers are obtained by self-supervised learning. The ANN can predict variations of the water level in the operational IW within respectable errors in under a second when correctly trained on synthetic data. In the next sections, the principles behind LSTM network will be covered as well as the FEM used to construct the synthetic data set. The methodology proposed in this work is finally illustrated through an application on an operational data set.

LONG SHORT-TERM MEMORY NETWORK

LSTM network is a variety of recurrent neural network (RNN) and can be perceived as successive copies of the same ANN connected through time via hidden state variables (Olah, 2015). In other words, information at the current time step is connected to the next prediction task. Cells state is the main component in a LSTM cell as it stores relevant long-term dependencies rather than carrying it along over time steps like RNNs (Goodfellow *et al.,* 2016). LSTM cells also learn to decide when to self-reset their memory, based on the input sequence, thus making them adaptive even once trained (Gers *et al.,* 1999). As shown in Figure 1, a LSTM cell has four learned neural network layers (yellow boxes), consisting of three sigmoid layers and a hyperbolic tangent layer. The sigmoid layers act as regulation gates for the cell and hidden state as they filter the relevant (or irrelevant) information to be passed (or retained) to the next time step. Values are squeezed between 0 and 1 in a vector of length corresponding to the dimensionality of the cell state, where

more information is added (or removed) as values get closer to 1. The hyperbolic tangent layer, on the other hand, proposes new information to be added to the cell state via an output vector with values constrained in the range [-1, 1].

The updated cell state ($\mathbf{c}_t$) results in a series of additions and/or subtractions on the cell state of the previous time step ($\mathbf{c}_{t-1}$). The forget gate ($\mathbf{f}_t$) determines what portion of the past cell state ($\mathbf{c}_{t-1}$) is irrelevant and should be deleted given the current variables ($\mathbf{x}_t$) and the past hidden state ($\mathbf{h}_{t-1}$). Writing new relevant information in the cell state is dictated by the input gate ($\mathbf{i}_t$) and the candidate values ($\tilde{\boldsymbol{c}}_t$). The updated hidden state ($\mathbf{h}_t$), which is also the output of the LSTM cell, is subsequently updated with a subset of the updated cell state that has been previously filtered by the output gate ($\mathbf{o}_t$) and passed through a hyperbolic tangent function, so that only relevant information is used for prediction at this time step. This process is then repeated for each time step in the sequence (Olah, 2015).

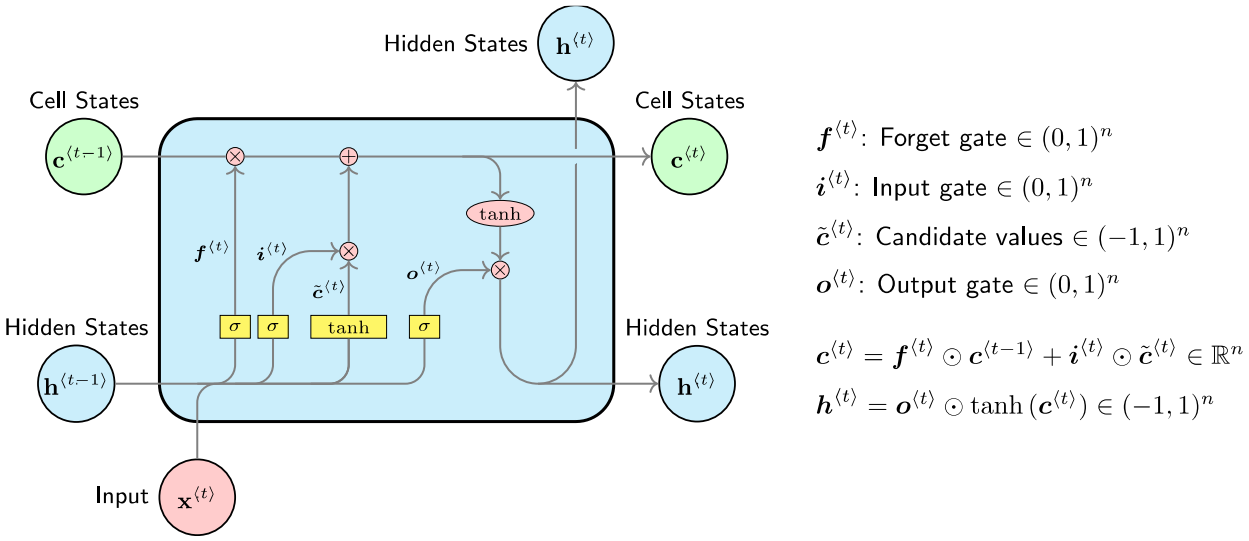

Figure 1 The structure of a typical LSTM cell where σ is a sigmoid layer, tanh (yellow) is a hyperbolic tangent layer, and where tanh (red) is the hyperbolic tangent function applied to a scalar. Note that $\odot$ is the Hadamard product, n denotes the size of the cell and hidden state vectors.

CONSTRUCTION OF A TRAINING SET WITH A NUMERICAL MODEL

ANNs require large operational data sets to achieve acceptable prediction performance. Operational data being often difficult to obtain, one way to overcome this constraint is to build a training set using a FEM. Rigorously built FEMs can be quite computationally expensive and they most likely require field work to validate the model with experimental data. Since building a large synthetic data set can also be time consuming, the FEM used to train the network needs not to be as accurate as a numerical model used for prediction purposes. The LSTM network uses the FEM's inputs and output times series to learn non-linear and non-stationary physical processes.

Heat Transfer and Groundwater Flow Model

A simplified 2D-axisymmetric FEM in the COMSOL Multiphysics environment (COMSOL, 2021) is commonly used to couple groundwater flow and heat transfer to emulate a single SCW's operation and limit computation time (Beaudry *et al.*, 2018, 2019; Eppner *et al.*, 2017; Nguyen *et al.*, 2015). In this study, the validated model developed by Beaudry *et al.* (2019) to emulate an operational SCW connected to a geothermal laboratory has been modified to represent the geometry of the IW, that is also present on the study site (see Table 1). Note that the final depth of the reinjection pipe

corresponds to the mid-point of its perforated section. During the model's development, care was taken to ensure that lateral boundary conditions were not significantly affecting the hydraulic heads and temperatures of the fluid returned to the IW. The domain is discretized into 5472 quadratic elements.

Table 1. Numerical Model's Geometry

Parameters	Clayey Silt	Rock	Injection Well	Reinjection Pipe
Depth	3 m	152 m	152 m	130 m
Radius	30 m	30 m	83 mm	24.34 / 30.16 mm

Table 2 presents the properties of the four materials composing the IW and its surroundings. Water density and water dynamic viscosity were set as temperature-dependent variables in the model, which allows variations of hydraulic conductivity through time. One could refer to Beaudry *et al.* (2019) for a thorough description of the experimental site and numerical model. Note that hydraulic and thermal properties of the bedrock were drawn, for each simulation, from uniform distributions. This was done to illustrate the fact that even if local properties are quite uncertain, a well-trained LSTM network can reproduce accurately operational measurements.

Table 2. Numerical Model's Parameters

Parameters	Unit	Clayey Silt	Rock	HDPE Pipe	Water
Porosity	-	0.2	0.01	0	-
Hydraulic Conductivity	ms^{-1}	10^{-7}	$[3.5, 4.1]\times10^{-7}$	10^{-9}	-
Specific storage	m^{-1}	10^{-3}	$[0.9, 1.1]\times10^{-5}$	4×10^{-6}	4×10^{-6}
Volumetric heat capacity	$MJm^{-3}K^{-1}$	1.4	[1.8, 2.2]	2.17	4.18
Thermal conductivity	$Wm^{-1}K^{-1}$	1.8	[2.5, 3.0]	0.42	0.59

Figure 2a illustrates the IW's geometry and the model's boundary conditions. One should note that an unspecified boundary condition indicates that a zero-flux boundary is set. The initial hydraulic head ($H_{t=0}$) of the model and the lateral boundary is fixed to 150 m relative to the model's base. The inflow boundary ($v_{t,in}=V_{t,in}/A_{in}$) at the top of the IW is set as a time-varying stepwise function that includes the flow rate ($V_{t,in}$) and the cross-sectional area of the injection pipe (A_{in}). The initial temperature of the domain and the lateral boundary corresponds to a temperature profile (T_z) measured in the IW. The water temperature ($T_{t,in}$) and air temperature ($T_{t,air}$) are time-varying functions implemented in the model. Natural heat flux (q_{geo}) is fixed at the base of the model to 0.063 Wm^{-2} and was obtained with the geothermal gradient and the thermal conductivity following the relation $q_{geo}=k\cdot dT/dz$.

Simulation Strategy

Once the FEM was built and operational, a total of 500 simulations were carried out to obtain the IW's hydraulic response under different flow rate ($V_{t,in}$) and inlet temperature ($T_{t,in}$) time series. The FEM was simulated over a period of 36 days (864 hours) with a time step of 5 minutes. Hence, the length of every sequence forming the training set is 10369 steps. The 500 simulations were performed with thermal parameters (thermal conductivity and volumetric heat capacity) and hydraulic parameters (hydraulic conductivity and specific storage) drawn from the bounded uniform distributions shown in Table 2. A new time-varying function of inlet temperature ($T_{t,in}$) and flow rate ($V_{t,in}$) was used for each simulation. An example is shown in Figure 2b and 2c. The approach consisted of generating flow rate ($V_{t,in}$) and specific heat load (q) time series with values randomly sampled from 0, 6.67, 13.33 and 20 L/min and from 0, 25, 50 and 75 W/m. The length of the step intervals was also drawn following a uniform distribution from 2, 4, 6, 9, 12 and 18 days. The inlet temperature ($T_{t,in}$) was then derived from the infinite line-source model (Ingersoll *et al.*, 1954) using specific heat load (q) time series and corresponding thermal parameters. This approach allowed us to approximate the outlet temperature at the SCW, which was then used as the inlet temperature ($T_{t,in}$) at the IW while leaving the SCW out of the FEM and thus, speeding up simulation time. Assembling the complete training set required approximately 12.5 days on a quite busy server. An additional independent simulation was generated to assess the accuracy of the network.

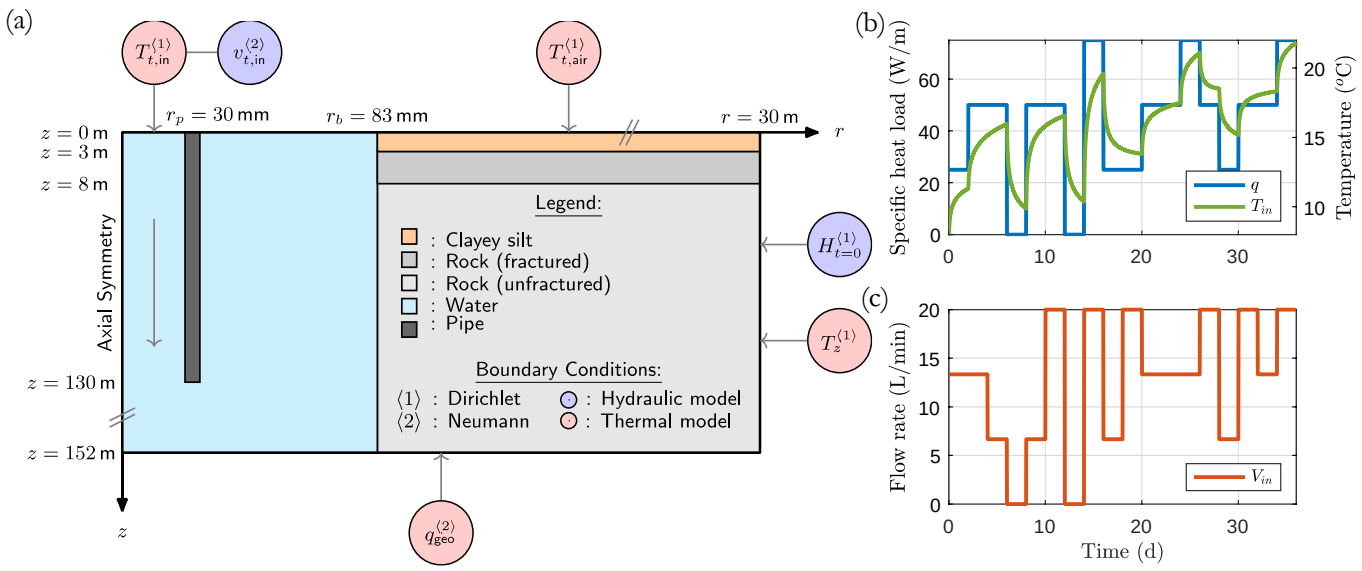

Figure 2 (a) Geometry and boundary conditions of the coupled numerical model used to generate the training data set. If unspecified, a zero-flux boundary is used (not to scale). (b) Generated specific heat load (q) stepwise function and corresponding injected water temperature ($T_{t,in}$) derived from the infinite line-source model used in the fifth simulation. (c) Flow rate ($V_{t,in}$) time series implemented in the fifth simulation.

PROPOSED LSTM NETWORK

In this study, the neural network was built using the Deep Learning Toolbox of MATLAB (MATLAB, 2021). Weights and biases of each layer in the network are modified at every iteration in the training phase to minimize an objective function (Goodfellow *et al.,* 2016). The optimal framework was identified as the one minimizing the mean squared error (MSE) and the root-mean-squared error (RMSE) on an independent synthetic validation set to prevent overfitting the data to the training set. LSTM networks with one to four layers combined with various activation layer (sigmoid, rectified linear unit and hyperbolic tangent) and regularization layer (dropout, layer normalization, batch normalization) were tested. Hyperparameters, such as the number of hidden units in each LSTM layer, initial learning rate and dropout probability were optimized using Bayesian optimization. Prior to training, inputs and outputs were rescaled to be in the range [-1, 1]. Such normalization is a standard practice as it accelerates the learning process with gradient-based algorithms (LeCun *et al.*, 2012). Flipping, a data augmentation technique, was used to improve performance prediction of the LSTM network (Wen *et al.*, 2021). Table 3 displays the parameters used to train the optimal LSTM network obtained from Bayesian optimization.

Table 3. Parameters for training the LSTM Network

Parameters	Value	Parameters	Value
Number of hidden layers	4	Epochs	10
Initial learning rate	0.0003	Mini-batch size	25
Learning rate drop factor	0.9	Loss function	MSE
Learning rate drop period	1	Optimizer	Adam
Dropout rate	0.2	Activation function	tanh

The optimal architecture, as illustrated in Figure 3, consists of an input layer, four hidden layers, that includes three LSTM layers, a fully connected layer, and an output layer. Layer normalization and dropout are the regularization techniques applied to the LSTM network. These layers prevent the neural network from overfitting, improve its

prediction performance and decrease training time (Ba *et al.*, 2016; Srivastava *et al.*, 2014). To ease the learning process, the network was trained to reconstruct $s_t/(V_{t,in}+1)$, that is the negative drawdown divided by the flow rate plus one. The output was then transformed back to s_t. This transformation prevented problems associated with fast-changing water levels and division by zero (zero flow rate). Training and validation sets were displaying a loss function (MSE) having an asymptotic behavior and a similar value at the end of the training phase, hence indicating good generalization from the trained network. The LSTM network allows negative drawdown prediction in the IW within an RMSE of 10.9 cm with respect to the synthetic validation time series.

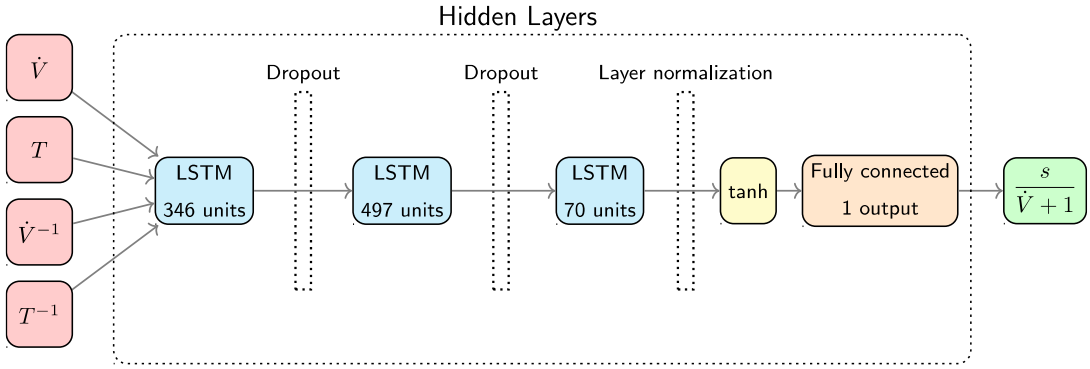

Figure 3 Architecture of the proposed LSTM network. Inputs are the flow rate and inlet temperature, as well as the inverse of their time series. The output is the negative drawdown divided by the flow rate plus one.

PERFORMANCE PREDICTION ON AN OPERATIONAL DATA SET

The operational data set used in this study was gathered by the geothermal laboratory of Polytechnique Montréal. The laboratory, now located in Varennes, Canada, is connected to a 215 m deep SCW and a 152 m deep IW located 10 m apart from each other in a moderately permeable bedrock (Beaudry *et al.,* 2018, 2019). Respectively, a variable speed submersible pump, an energy valve and a 24-kW water heater control the pumping rate, the bleed ratio, and the groundwater temperature. One should refer to Beaudry *et al.* (2018, 2019) for a comprehensive hydrogeothermal characterization and Cerclet *et al.* (2020) for details concerning equipment and sensors installed at the geothermal laboratory.

The predictive performance of the LSTM network was tested on a 36-day operation test conducted in summer 2019 at the geothermal laboratory. Figure 4a illustrates the monitored inlet and outlet temperature along with matching ground thermal loads during the experiment. Pumping rates in the SCW and discharge flow rates in the IW are also shown in Figure 4b. Multiple heating and recovery phases occurred during the experiment with heating power ranging from 0 to 24 kW (112 W/m). The operation was performed with two bleed periods where discharge flow rates were set at 7.5 L/min and 15 L/min (bleed ratio of 10%). Flow rates were recorded with a time step interval of 1 minute by an energy valve located inside the laboratory and having a 2 % accuracy. The water level in the IW was initially located at a depth of 1.8 m and was monitored in the annular space of the IW with a time step interval of 1 minute using a pressure sensor displaying an accuracy of 0.5 cmH_2O. The same probe contained a temperature sensor which recorded water temperatures with a 0.1 °C accuracy. A spline interpolation, for a time step of 5 minutes, and a low-pass filter were applied on the measurements to remove high-frequency noise.

The forecasted drawdown along with the operational measurements are illustrated in Figure 5. Results indicate a very good match during the first 18 days with an RMSE of 14.8 cm. Notice how the heads, and the underlying effect of

temperature, are well reproduced by the LSTM network between days 12 and 18 (RMSE of 7.3 cm). We will show below that the proposed neural network exhibits the expected predictive behavior regarding flow rate and inlet temperature. As one can notice, overflowing occurred in the IW between days 27 and 35 of the experiment when the discharge rate was set at 15 L/min. This is a clear example of a previously mentioned problem related to IW in GSHP system. Also, between the two bleeding periods, a positive drawdown is observed in the IW. Natural fluctuation of the water level from greater evapotranspiration and less recharge is a plausible explanation to this observation. Both wells being only 10 m apart, hydraulic interaction between the SCW and the IW might have contributed as well to the measured drawdown. The 2D-axisymmetric FEM used to train the LSTM network did not take into consideration natural factors affecting water levels nor the SCW, thus explaining the incapability of the ANN to accurately forecast this segment (RMSE of 30.4 cm). Nevertheless, for the first 18 days of the experiment, the predicted drawdown and the one observed during the experiment are in good agreement.

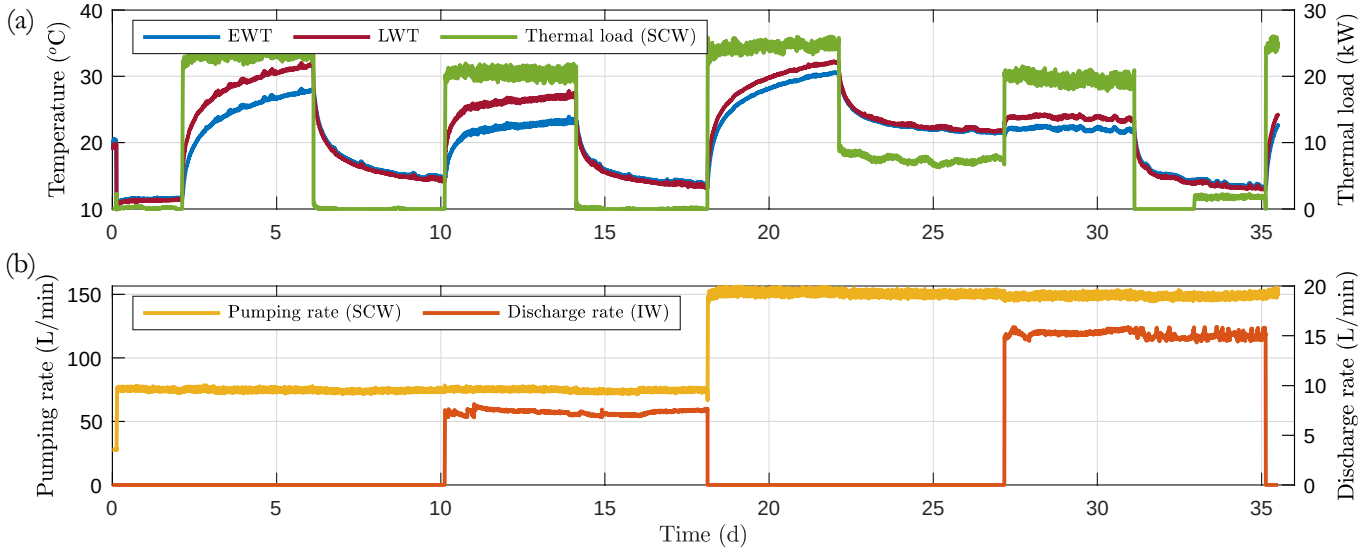

Figure 4 (a) Monitored entering water temperature (EWT), leaving water temperature (LWT) temperature and thermal load imposed to the 215-m SCW. (b) Recorded pumping rate in the SCW and discharge rate in the IW.

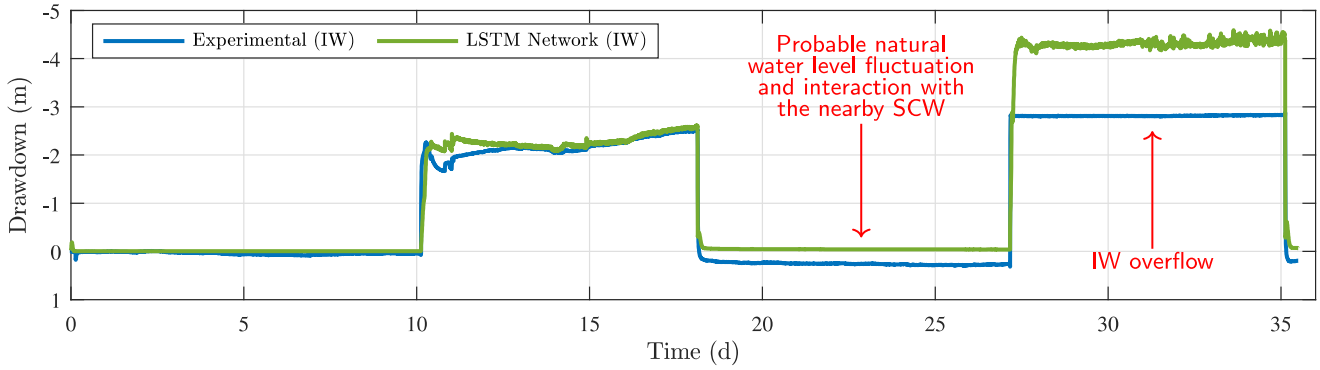

Figure 5 Operational measured drawdown in the IW and predicted drawdown by the LSTM network.

FURTHER RESULTS AND DISCUSSION

The impact of flow rate and inlet temperature on the forecasted drawdown has been studied to determine whether outputs displayed expected behaviors regarding water level variations and whether the proposed LSTM network could take into consideration the effect of temperature on hydraulic conductivity. To do so, different constant flow rates (2, 6, 10, 14 and 18 L/min) were fed to the LSTM network while using the same inlet temperature time series (see Figure 6a). The comparison is shown in Figure 6b.

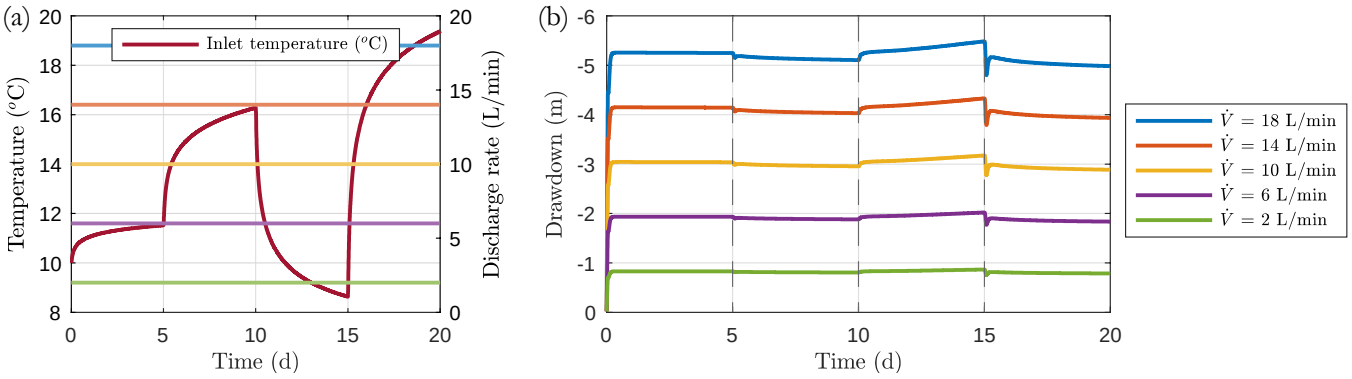

Figure 6 (a) Flow rates ($V_{t,in}$) and the inlet temperature ($T_{t,in}$) used to study their impact on drawdowns predicted by the LSTM network. (b) Drawdowns predicted by the LSTM network.

First and foremost, results show that forecasted negative drawdown in the IW increases proportionally with flow rates. Following Darcy's law for fluid flow in porous media (Darcy, 1856), analogous to Fourier's law of heat conduction (Fourier, 1878), drawdowns are supposed to vary proportionally with flow rates. Hence, predictions of the proposed LSTM network display the expected behavior with respect to flow rates. Furthermore, for an increasing inlet temperature, negative drawdown in the well should decrease as the hydraulic conductivity of the aquifer increases. Inversely, as the inlet temperature lessens, negative drawdown is supposed to increase. As seen in Figure 6b, this behavior is also respected for all flow rates, although appearing more preeminent with high flow rates due to the scaling effect of the figure. For example, between days 10 and 15, the inlet temperature dropped from 16.3 °C to 8.6 °C. This temperature variation resulted in an increase of the negative drawdown by 7.4 % with respect to the initial drawdowns at day 10 and that, for all flow rates. It is worth mentioning that the variation of the negative drawdown is similar for any given time intervals and flow rates. Thus, the impact of the inlet temperature on the network's response is similar for all flow rates and the LSTM network do consider the effect of temperature.

CONCLUSION

In this paper, a LSTM network was trained using 500 synthetic time series generated with a FEM coupling heat transfer and groundwater flow to predict negative drawdown in the IW of a GSHP system. The predictive performance of the ANN was tested on a 36-day operation at the geothermal laboratory of Polytechnique Montréal. The resulting RMSE between the forecasted and measured negative drawdown is 14.8 cm. As of now, this method, which considers the effect of temperature on hydraulic conductivity, has demonstrated its prediction performance on a short-time operational data set. The proposed LSTM network is specific to a particular site as it currently lacks generalization capabilities to be extended to different well geometries and other sites. Comparative studies with other ANN methods such as RNN, convolution neural network, transformer neural network and Bayesian neural network should be carried out to improve and compare forecasting performance.

ACKNOWLEDGMENTS

The authors acknowledge the support from partners of the Geothermal Research Chair on the Integration of SCWs in Institutional Buildings, namely Hydro-Québec, the Ministry of Higher Education of Québec, CSSMI, CSSDM, CSSS, Versa Profiles, Marmott Energy, CanmetEnergy and NSERC. Additionally, we thank the anonymous reviewers and colleagues (L. Jacques, L. Champagne-Péladeau) that provided constructive comments. This work was financed by the Natural Sciences and Engineering Research Council of Canada through grant number ALLRP 544477-19.

REFERENCES

Ba, J. L., J. R. Kiros and G. E. Hinton. 2016. *Layer Normalization.* ArXiv:1607.06450.

Ballard, T. 2017. *Using Specific Capacity to Monitor Well Performance*. Southeast Hydrogeology.

Banks, D. 2012. An introduction to thermogeology: Ground source heating and cooling (2nd ed). John Wiley & Sons, Ltd.

Beaudry, G., P. Pasquier and D. Marcotte. 2018. *Hydrogeothermal characterization and modelling of a standing column well experimental installation.* Proceedings of the IGSHPA Research Track 2018.

Beaudry, G., P. Pasquier and D. Marcotte. 2019. *The impact of rock fracturing and pump intake location on the thermal recovery of a standing column well: Model development, experimental validation, and numerical analysis.* Science and Technology for the Built Environment, 25(8), 1052–1068.

Bouwer, H. 2002. *Artificial recharge of groundwater: Hydrogeology and engineering*. Hydrogeology Journal, 10(1), 121–142.

Cerclet, L., B. Courcelles and P. Pasquier. 2020. *Impact of Standing Column Well Operation on Carbonate Scaling*. Water, 12.

Cho, H. U., Y. Nam, E. J. Choi, Y.J. Choi, H. Kim, S. Bae and J. W. Moon. 2021. *Comparative analysis of the optimized ANN, SVM, and tree ensemble models using Bayesian optimization for predicting GSHP COP*. Journal of Building Engineering, 44.

COMSOL. 2021. *COMSOL Multiphysics* (6.0) [Computer software]. COMSOL AB.

Darcy, H. 1856. *Les fontaines publiques de la ville de Dijon: Exposition et application des principes à suivre et des formules à employer dans les questions de distribution d'eau : Ouvrage terminé par un appendice relatif aux fournitures d'eau de plusieurs villes, au filtrage des eaux et à la fabrication des tuyaux de fonte, de plomb, de tôle et de bitume.* V. Dalmont.

Dusseault, B. and P. Pasquier. 2018. *Near-instant g-function construction with artificial neural networks*. Proceedings of the IGSHPA Research Track 2018.

Dusseault, B. and P. Pasquier. 2019. *Efficient g-function approximation with artificial neural networks for a varying number of boreholes on a regular or irregular layout.* Science and Technology for the Built Environment, 25(8), 1023–1035.

Dusseault, B. and P. Pasquier. 2021. *Usage of the net present value-at-risk to design ground-coupled heat pump systems under uncertain scenarios*. Renewable Energy, 173, 953–971.

Eppner, F., P. Pasquier and P. Baudron. 2017. *A coupled thermo-hydro-geochemical model for standing column well subject to CO2 degassing and installed in fractured calcareous aquifers*. Geomechanics for Energy and the Environment, 11, 14–27.

Esen, H. and M. Inalli. 2009. *Modelling of a vertical ground coupled heat pump system by using artificial neural networks.* Expert Systems with Applications, 36(7), 10229–10238.

Fourier, J. B. J. 1878. *The analytical theory of heat*. Cambridge : University Press.

Gang, W., J. Wang and S. Wang. 2014. *Performance analysis of hybrid ground source heat pump systems based on ANN predictive control*. Applied Energy, 136, 1138–1144.

Gers, F. A., J. Schmidhuber and F. Cummins. 1999. *Learning to forget: Continual prediction with LSTM*. 1999 Ninth International Conference on Artificial Neural Networks ICANN 99. (Conf. Publ. No. 470), 2, 850–855 vol.2.

Gjengedal, S., R. Ramstad, B. Hilmo and B. Frengstad. 2019. *Fouling and clogging surveillance in open loop GSHP systems: A systematic procedure for fouling and clogging detection in the whole groundwater circuit.* Bulletin of Engineering Geology and the Environment, 79.

Gjengedal, S., R. K. Ramstad, B. O. Hilmo and B. Frengstad. 2018. *Video inspection of wells in open loop ground source heat pump systems in Norway*. Proceedings of the IGSHPA Research Track 2018.

Gjengedal, S., L.A. Stenvik, R. K. Ramstad, J. I. Ulfsnes, B. O. Hilmo and B. S. Frengstad. 2021. *Online remote-controlled and cost-effective fouling and clogging surveillance of a groundwater heat pump system.* Bulletin of Engineering Geology and the Environment, 80(2), 1063–1072.

Goodfellow, I., Y. Bengio and A. Courville. 2016. Deep Learning. The MIT Press.

Ingersoll, L. R., O. J. Zobel and A. C. Ingersoll. 1954. Heat conduction with engineering, geological and other applications. Wisconsin U.P.

LeCun, Y. A., L. Bottou, G. B. Orr and K.-R. Müller. 2012. *Efficient BackProp*. In Neural Networks: Tricks of the Trade (2nd ed.) (pp. 9–48). Springer.

MATLAB. 2021. *MATLAB* (Version R2021b) [Computer software]. The MathWorks Inc.

Nguyen, A., P. Pasquier and D. Marcotte. 2015. *Influence of groundwater flow in fractured aquifers on standing column wells performance.* Geothermics, 58, 39–48.

Olah, C. 2015. *Understanding LSTM Networks*. Colah's Blog.

Pasquier, P. and D. Marcotte. (2020). *Robust identification of volumetric heat capacity and analysis of thermal response tests by Bayesian inference with correlated residuals*. Applied Energy, 261.

Pasquier, P., A. Nguyen, F. Eppner, D. Marcotte and P. Baudron. 2016. *Standing column wells*. In Advances in Ground-Source Heat Pump Systems (pp. 269–294). Woodhead Publishing.

Pasquier, P., A. Zarrella. and R. Labib. 2018. *Application of artificial neural networks to near-instant construction of short-term g-functions*. Applied Thermal Engineering, 143, 910–921.

Puttige, A. R., S. Andersson, R. Östin and T. Olofsson. 2020. *A Novel Analytical-ANN Hybrid Model for Borehole Heat Exchanger.* Energies, 13(23).

Puttige, A. R., S. Andersson, R. Östin and T. Olofsson. 2021. *Application of Regression and ANN Models for Heat Pumps with Field Measurements*. Energies, 14(6).

Snijders, A. L. and B. C. Drijver. 2016. *Open-loop heat pump and thermal energy storage systems*. In Advances in Ground-Source Heat Pump Systems (pp. 247–268). Woodhead Publishing.

Srivastava, N., G. Hinton, A. Krizhevsky, I. Sutskever and R. Salakhutdinov. 2014. *Dropout: A Simple Way to Prevent Neural Networks from Overfitting*. Journal of Machine Learning Research, 15(56), 1929–1958.

Sun, W., P. Hu, F. Lei, N. Zhu and Z. Jiang. 2015. *Case study of performance evaluation of ground source heat pump system based on ANN and ANFIS models*. Applied Thermal Engineering, C(87), 586–594.

Wang, G., H. Wang, Z. Kang and G. Feng. 2020. *Data-Driven Optimization for Capacity Control of Multiple Ground Source Heat Pump System in Heating Mode*. Energies, 13(14).

Wen, Q., L. Sun, F. Yang, X. Song, J. Gao, X. Wang and H. Xu. 2021. *Time Series Data Augmentation for Deep Learning: A Survey*. Proceedings of the Thirtieth International Joint Conference on Artificial Intelligence, 4653–4660.

Xie, Y., P. Hu, N. Zhu, F. Lei, L. Xing, L. Xu. and Q. Sun. 2020. *A hybrid short-term load forecasting model and its application in ground source heat pump with cooling storage system*. Renewable Energy, 161, 1244–1259.

Xu, C. and H. Chen. 2020. *Abnormal energy consumption detection for GSHP system based on ensemble deep learning and statistical modeling method*. International Journal of Refrigeration, 114, 106–117.

Xu, C., H. Chen, J. Wang, Y. Guo and Y. Yuan. 2019. *Improving prediction performance for indoor temperature in public buildings based on a novel deep learning method*. Building and Environment, 148, 128–135.

Zhang, C., J. Li, Y. Zhao, T. Li, Q. Chen and X. Zhang. 2020. *A hybrid deep learning-based method for short-term building energy load prediction combined with an interpretation process*. Energy and Buildings, 225.

Zhou, S., J. Li, Y. Zhang, X. Liu and W. Zhang. 2021. *Prediction of the ground temperature variations caused by the operation of GSHP system with ANN*. Geothermics, 95.